Single shot x-ray phase contrast imaging using a direct conversion microstrip detector with single photon sensitivity

Kagias, M ; Cartier, S ; Wang, Z ; Bergamaschi, A ; Dinapoli, R ; Mozzanica, A ; Schmitt, B ; Stampanoni, M

DOI: https://doi.org/10.1063/1.4948584

AIP Applied Physics Letters

Single shot x-ray phase contrast imaging using a direct conversion microstrip detector with single photon sensitivity

M. Kagias, S. Cartier, Z. Wang, A. Bergamaschi, R. Dinapoli, A. Mozzanica, B. Schmitt, and M. Stampanoni

Citation: Applied Physics Letters **108**, 234102 (2016); doi: 10.1063/1.4948584
View online: http://dx.doi.org/10.1063/1.4948584
View Table of Contents: http://scitation.aip.org/content/aip/journal/apl/108/23?ver=pdfcov
Published by the AIP Publishing

Single shot x-ray phase contrast imaging using a direct conversion microstrip detector with single photon sensitivity

M. Kagias,[1,2,a)] S. Cartier,[1,2,a)] Z. Wang,[1,2] A. Bergamaschi,[1] R. Dinapoli,[1] A. Mozzanica,[1] B. Schmitt,[1] and M. Stampanoni[1,2]
[1]*Swiss Light Source, Paul Scherrer Institute, 5232 Villigen, Switzerland*
[2]*Institute for Biomedical Engineering, University and ETH Zurich, 8092 Zurich, Switzerland*

(Received 10 February 2016; accepted 20 April 2016; published online 7 June 2016)

X-ray phase contrast imaging enables the measurement of the electron density of a sample with high sensitivity compared to the conventional absorption contrast. This is advantageous for the study of dose-sensitive samples, in particular, for biological and medical investigations. Recent developments relaxed the requirement for the beam coherence, such that conventional X-ray sources can be used for phase contrast imaging and thus clinical applications become possible. One of the prominent phase contrast imaging methods, Talbot-Lau grating interferometry, is limited by the manufacturing, alignment, and photon absorption of the analyzer grating, which is placed in the beam path in front of the detector. We propose an alternative improved method based on direct conversion charge integrating detectors, which enables a grating interferometer to be operated without an analyzer grating. Algorithms are introduced, which resolve interference fringes with a periodicity of 4.7 μm recorded with a 25 μm pitch Si microstrip detector (GOTTHARD). The feasibility of the proposed approach is demonstrated by an experiment at the TOMCAT beamline of the Swiss Light Source on a polyethylene sample. *Published by AIP Publishing.*
[http://dx.doi.org/10.1063/1.4948584]

X-ray grating interferometry (GI) is capable of providing simultaneously three complementary contrasts: absorption, differential phase, and small-angle scattering.[1–3] The differential phase signal can reveal differences between materials with similar absorption properties since it is highly sensitive to the electron density variations of the sample. The small-angle scattering signal, also known as dark-field, is able to access unresolved structural variations of the sample in the (sub) micrometer scale which are beyond the resolution capability of the imaging modality. Both the differential phase and the dark field signals have been demonstrated to be capable of providing valuable information additional to the traditional absorption contrast in medical imaging,[4–6] material science, and non-destructive testing.[7]

Early phase contrast imaging (PCI) techniques were developed for synchrotron facilities due to the required high beam coherence.[8,9] It was not until the development of the Talbot-Lau grating interferometer (GI)[10] and later the coded aperture[11] that measuring phase signals with conventional X-ray tubes became feasible. The Talbot-Lau grating interferometer consists of three gratings: an absorption grating G_0 placed close to the source that intends to increase the spatial coherence of the source, a phase grating G_1 that produces an interference pattern at a certain distance downstream (Talbot effect), and finally, a second absorption grating G_2 which is placed at a selected Talbot distance right in front of the detector to sample the periodic signal with a sub-pixel spatial frequency. When a sample is introduced into the beam, it will cause distortions to the interference pattern due to X-ray absorption, refraction, and small-angle scattering. These distortions can be sensed by the so-called phase stepping procedure[1] in which G_2 is scanned step by step for one or more periods. At each step, an image is recorded which results in an intensity curve at each pixel. The absorption, differential phase, and small-angle scattering signals can be extracted from two phase stepping curves obtained with and without the sample. Although the utilization of G_2 decouples the sensitivity of the interferometer from the detector resolution, it comes at the price of a lower system dose efficiency due to the photon absorption it introduces. Additionally, phase stepping introduces extra mechanical complexity to the system and increased scanning time. Finally, a strict set of requirements concerning G_2 renders the successful manufacturing challenging.[12,13] Specifically, the two limiting factors at the moment are the area and the aspect ratio of the gratings. Medical applications require large imaging field of views (hundreds of square centimeters) which means that dense microstructures have to be produced over a large area with a high uniformity in terms of depth, duty cycle, and period. Nonetheless, to meet the criteria for high phase sensitivity at higher energies, the aspect ratio of the absorbing structures increases dramatically. All of these indicate that a G_2-less interferometer has the potential to increase the applicability of PCI.

In this letter, we show that G_2 can be omitted (G_2-less) when using a charge integrating direct conversion detector where inter-pixel interpolation can be performed (works only for small pitches) and therefore the PCI setup can be significantly simplified. Our approach renders the phase stepping procedure unnecessary and results in a single shot PCI method.[14–21] Compared to other single shot grating based PCI methods,[22,23] ours does not compromise the system sensitivity as it exploits much smaller fringe pitch (smaller than the physical detector pixel size). The chosen detector,

[a)]M. Kagias and S. Cartier contributed equally to this work.

GOTTHARD, is a microstrip detector with a strip pitch of 25 μm and single photon sensitivity down to ~2.7 keV photon energy.[24] It is possible to resolve the fringes produced by G_1 down to a 4.7 μm pitch directly. This is accomplished by single photon detection and appropriate analysis of the generated charge values which allows the estimation of the photon position beyond the detector channel size.[25] However, the achievable resolution is spatially modulated within each channel pair; for this reason, we developed a phase retrieval algorithm exploiting the Hilbert transform (HT) which allows the analysis of such signals. The proposed method was demonstrated experimentally at the synchrotron.

A G_2-less grating interferometer consists of a phase grating (G_1) placed directly after the sample and a strip detector placed downstream at a Talbot distance (see Fig. 1). By scanning the sample vertically through the X-ray beam, it is possible to acquire a two-dimensional image. To enhance the image resolution in the scanning direction, the beam is collimated by a 2 μm tungsten slit in front of the detector.

The GOTTHARD detector uses direct conversion sensors, in which X-ray photons are absorbed in the sensor (typically silicon) and produce electron-hole pairs in the semiconductor with a conversion coefficient of 1 e^-/3.62 eV.[26] The sensor is biased, such that the electrons drift toward the read-out electrodes, where the signal is collected, amplified, and then integrated in the read-out chip of the detector. The initial point-like electron cloud produced at the point of interaction broadens during the transport through the sensor and has an average diameter of 17 ± 3 μm (Ref. 27) at the collection surface of a 320 μm thick silicon sensor. The charge generated from one absorption event is collected by more than one channel for small channel sizes (i.e., in the order of the electron cloud diameter), which is known as charge sharing.[28] If the photon flux is low compared to the frame rate, meaning that the detected photons during the acquisition of a frame are very few, single photon absorption events are separable and can be analyzed individually by evaluating the signal height of adjacent channels. In this single photon regime, the charge integrating circuit allows to determine the energy of the absorbed photon and the interaction position can be retrieved down to a few microns. Repeating this process for many photons allows the acquisition of a high resolution image.[25]

The G_2-less PCI experiment consists of three measurements: the blank measurement (no G_1, no sample) for position reconstruction calibration, the grating measurement (with G_1 only) as a reference for the phase retrieval algorithm and the sample measurement, where both G_1 and the sample are present in the beam. The blank measurement and the grating measurement just need to be done once if the setup and measurement parameters do not change.

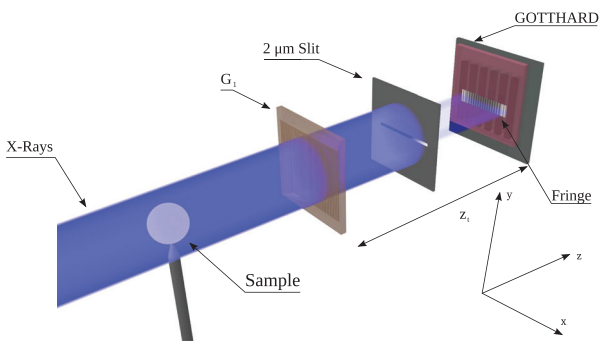

FIG. 1. Setup of the G_2-less grating interferometer. The microstrip detector is placed at a distance of $z_t = 15$ cm downstream of G_1. The microstrips have a length of several mm, and therefore, the beam is additionally collimated by a 2 μm tungsten slit directly in front of the sensor.

After acquisition, the frames containing single photon events are post processed to extract photon hits and to determine their positions. Each channel is divided into several virtual channels and the extracted photon hits are assigned to the virtual channels according to their position.

The first step of post-processing is the dark image correction, where a base signal is subtracted from the captured frames accounting for leakage current flowing through the sensor during acquisition. After that, the absorption events are identified if the signal value of a pair of channels exceeds a threshold. For each event n, the adjacent channels' pulse height denoted L_n (left neighbour) and R_n (right neighbour) and the channel index of the left channel c (identifying the channel couple) are extracted. The sum of L_n and R_n is proportional to the photon energy, and the ratio between the values is a non-linear representation of the photon absorption position. To linearise the absorption position, we use the η algorithm, a method first used in particle physics[29] and later demonstrated with X-rays in direct conversion detectors.[25,30] The η_n value for each event n is defined as $R_n/(L_n + R_n)$. The distribution $\mathrm{d}N/\mathrm{d}\eta$ of the η values is calculated from the blank measurement, where N is the total number of detected events. For each event of the sample measurement or the grating measurement, the interpolated position of the absorption location is calculated by

$$x^c(\eta_n) = p\frac{\int_{-\infty}^{\eta_n}\frac{\mathrm{d}N}{\mathrm{d}\eta}\mathrm{d}\eta}{\int_{-\infty}^{\infty}\frac{\mathrm{d}N}{\mathrm{d}\eta}\mathrm{d}\eta}, \tag{1}$$

where p is the size of a detector channel. The reconstructed high resolution intensity signals of the grating measurement and sample measurement (denoted by $I_g^c(x)$ and $I_s^c(x)$) correspond to the distribution $\mathrm{d}N/\mathrm{d}x^c$ of events in the x-dimension of the channel pair c. The intensity signals $I_g^c(x)$ and $I_s^c(x)$ are sampled with the number of virtual channels N_x and a uniform spatial sampling rate of N_x/p as illustrated in Fig. 2.

The aim of the proposed phase retrieval method is to extract the differential phase value for each channel pair. This task exhibits two major challenges when compared to standard single shot Fourier based phase retrieval methods.[22,23] First, under general imaging conditions, the physical size of a detector channel p (25 μm in our case) will not be a multiple of the projected fringe period, which is a limitation for Fourier based methods. Second, the resolution enhancement is not uniform between two detector channels due to non-linear charge sharing, and this results in a spatial modulation of the visibility of the recorded fringe as seen in Fig. 2. Therefore, more elaborate phase retrieval methods are required. We propose an algorithm that is able to determine the average phase shift of the most prominent frequency in a channel couple. The recorded interference fringe of the channel pair c can be approximated by

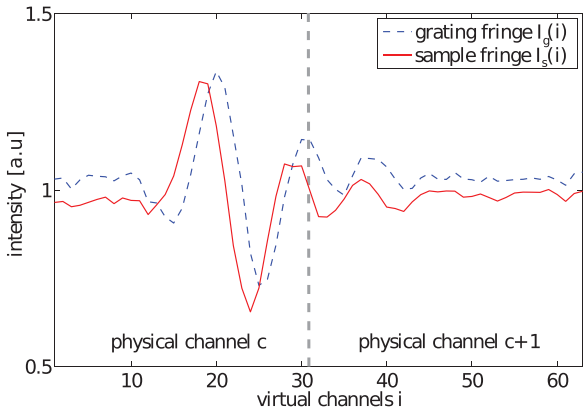

FIG. 2. Reconstructed intensity signals for a channel couple c. The exact channel is marked in yellow in Fig. 3(a). The detector resolution depends on the inter-channel position x and is in theory highest at the boundary between two channels. The high resolution region (and also the region with the highest fringes amplitude) is shifted to the left due to the potential misalignment of the detector with respect to the beam direction.

$$I^c(x_i) = a^c(x_i) + b^c(x_i)r^c(x_i)\cos(2\pi f_1 x_i - \phi^c(x_i)), \quad (2)$$

where x_i is the position of the virtual channel i, $i \in \mathbb{N}$ with $1 \le i \le N_x$, f_1 is the main frequency of the fringe, $a^c(x_i)$ is the sample absorption, and $b^c(x_i)$ and $\phi^c(x_i)$ represent the scattering factor and phase shift. The sample-independent term $r^c(x_i)$ is used to model the non-uniform resolution of a channel pair c. Specifically, it takes into account the localized visibility reduction (contrast loss) of the interference fringe as seen in Fig. 2. Assuming the absorption term is constant within a channel pair (i.e., $A^c = \frac{1}{N_x}\sum_{i=1}^{N_x} I_c(x_i)$), we can determine the dc-offset corrected signal

$$\tilde{I}^c(x_i) = I^c(x_i) - A^c = b^c(x_i)r^c(x_i)\cos(2\pi f_1 x_i - \phi^c(x_i)). \quad (3)$$

We obtain the complex *analytical signal* by adding the Hilbert transformed signal as the imaginary part

$$\hat{I}^c(x_i) = \tilde{I}^c(x_i) + i\mathcal{H}(\tilde{I}^c(x_i)). \quad (4)$$

$\hat{I}^c(x_i)$ encodes the instantaneous phase of the fringe $\phi^c(x_i)$ as the angle and the modulated instantaneous scattering factor $b^c(x_i)r^c(x_i)$ as the magnitude. For each channel couple c, the differential phase can be extracted from $\hat{I}_f^c(x_i)$ and $\hat{I}_s^c(x_i)$

$$P^c = \sum_{i=1}^{N_x} w(x_i)\arg\left\{\frac{\hat{I}_s^c(x_i)}{\hat{I}_g^c(x_i)}\right\}, \quad (5)$$

where $w(x_i)$ is a weighting function accounting for the non-uniform resolution of the reconstruction method with $\sum_{i=1}^{N_x} w(x_i) = 1$. In our case, $w(x_i)$ was chosen as a Gaussian curve with $\sigma = 1/\sqrt{2}\,\mu$m.

The presented experiments were performed at the TOMCAT beamline at the Swiss Light Source, Villigen, Switzerland.[31] The Si(111) monochromator was set to 16.7 keV. The beam was attenuated by a 50% filter and a 350 μm aluminum sheet to enter the single photon regime. A silicon $\pi/2$ phase grating (produced at the Laboratory for Micro and Nanotechnology (LMN) of the Paul Scherrer Institute, Villigen, Switzerland) with a pitch of 4.7 μm was placed behind the sample of investigation. The GOTTHARD detector was mounted at the first Talbot distance (15 cm) behind the phase grating. The 1280 microstrips of the read-out chip of the detector were coupled to an equally segmented 320 μm thick silicon sensor, which gives a detection efficiency of 59% at the X-ray energy of 16.7 keV. GOTTHARD can readout a selected region of 256 strips at 140 kHz frame rate. In the experiment, a region of 31 strips with a pitch of 25 μm was used. This corresponds to a field-of-view of 775 μm. Each channel was subdivided into 64 virtual channels. The investigated sample was a polyethylene (PE) sphere (Cospheric LLC, Santa Barbara, CA 93160, USA) with a diameter of 625 μm mounted on the tip of a steel needle. Two-dimensional image data were acquired by scanning the object vertically through the beam in 30 steps of $q = 25\,\mu$m. Fifty millions frames of an exposure time of 1 μs were acquired per measurement, resulted in a total scan time of about 3 h per image. This very long exposure time is mainly given by the long dead time determined by the low flux required by the detector to perform interpolation on single photons.

After the position interpolation, the sample intensity curve (i.e., $I_s^c(x)$) and the grating intensity curve (i.e., $I_g^c(x)$) were obtained for each channel pair c. The absorption and differential phase values were then calculated by using the proposed algorithm for each channel couple individually. The final images have a size of 30×30 *pixel*^{2} (Figs. 3(a) and 3(b)). The theoretical differential phase value for slice w and channel c (depicted in Fig. 3(c)) can be calculated by

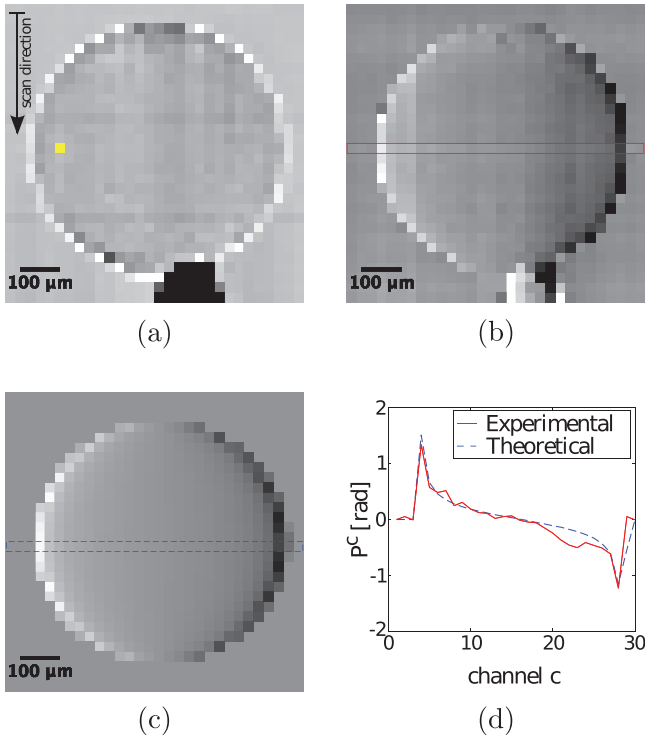

FIG. 3. Polyethylene sphere of 625 μm diameter acquired with the proposed method. (a) Absorption signal A^c, (b) differential phase signal P^c, and (c) calculated differential phase signal. (d) Comparison of experimental and theoretical signal calculated using (6) of the line profile indicated in (b) and (c).

$$P_t(c,w) = 4\pi \frac{\delta z_t}{g_1} \frac{(cp - 30p/2)}{\sqrt{r^2 - (cp - 30p/2)^2 - (wq - 30q/2)^2}}, \tag{6}$$

where $\delta = 8.1631 \times 10^{-7}$ for polyethylene at 16.7 keV, z_t is the distance between the phase grating and the detector, g_1 is the pitch of the phase grating, and r is the radius of the sphere. Fig. 3(d) compares the measured and theoretical differential phase profile calculated using Equation (6) for one image line, indicating that the proposed method can retrieve the differential phase information quantitatively.

Unfortunately, the photons absorbed in the center of a strip cause no or little charge sharing, and therefore, the resolution on their positions is worse than the grating's spatial frequency. This reduces the detection efficiency for the phase shift, but not for absorption. A more effective exploitation of all photons for detecting the phase shift and increase in the maximum spatial resolution can be achieved by enhancing the charge sharing, which is larger at lower energies (with the disadvantage that the radiation dose is increased as well) or can be obtained by an optimization of the detector by using smaller strip pitches, thicker sensors (which also increases the absorption efficiency), or the use of lower bias voltages to the sensors.[32] These last expedients will increase the diffusion time for the charge generated by the photons absorbed closer to the backplane, but will not affect the ones absorbed deeper in the sensor bulk, which are still a considerable amount at the energy used in our experiment. Spatial resolution is also affected by the alignment of the sensor compared to the X-ray beam due to the parallax given by the different depth of absorption of the 16.7 keV photons through the 320 μm silicon sensor ($\sim$300 nm per 1 mdeg misalignment).

In summary, we experimentally show that a single shot phase contrast imaging without the utilization of the analyzer grating (G_2) can be achieved by using a charge integrating direct conversion detector. We show that it is possible to retrieve quantitative differential phase information albeit the interference fringe is sampled in a less optimal way compared to the phase stepping method. As next steps, we plan to quantitatively measure the dose reduction in comparison with a conventional Talbot-Lau grating interferometer, test the performance of our method on conventional X-ray tubes, and extend to two-dimensional detector and two-dimensional gratings.

We thank G. Mikuljan, A. Astolfo, and F. Marone from Paul Scherrer Institute for their supports in the experiments and also the SLS detector group. Part of this work has been supported by the ERC Grant ERC-2012-StG 310005-PhaseX.

[1]T. Weitkamp, A. Diaz, C. David, F. Pfeiffer, M. Stampanoni, P. Cloetens, and E. Ziegler, Opt. Express **13**, 6296 (2005).
[2]A. Momose, S. Kawamoto, I. Koyama, Y. Hamaishi, K. Takai, and Y. Suzuki, Jpn. J. Appl. Phys., Part 2 **42**, L866 (2003).
[3]C. David, B. Nöhammer, H. H. Solak, and E. Ziegler, Appl. Phys. Lett. **81**, 3287 (2002).
[4]M. Stampanoni, Z. Wang, T. Thüring, C. David, E. Roessl, M. Trippel, R. A. Kubic-Huch, G. Singer, M. K. Kohl, and N. Hauser, Invest. Radiol. **46**, 801–806 (2011).
[5]D. Stutman, T. J. Beck, J. Carrino, and C. O. Bingham, Phys. Med. Biol. **56**, 5697–5720 (2011).
[6]T. Thüring, R. Guggenberger, H. Alkadhi, J. Hodler, M. Vich, Z. Wang, C. David, and M. Stampanoni, Skeletal Radiol. **42**(6), 827–835 (2013).
[7]V. Revol, I. Jerjen, C. Kottler, P. Schutz, R. Kaufmann, T. Luthi, U. Sennhauser, U. Straumann, and C. Urban, J. Appl. Phys. **110**, 044912 (2011).
[8]D. Chapman, W. Thomlinson, R. E. Johnston, D. Washburn, E. Pisano, N. Gmür, Z. Zhong, R. Menk, F. Arfelli, and D. Sayers, Phys. Med. Biol. **42**, 2015 (1997).
[9]A. Snigirev, I. Snigireva, S. Kohn, S. Kuznetsov, and I. Schelokov, Rev. Sci. Instrum. **66**, 5486 (1995).
[10]F. Pfeiffer, T. Weitkamp, O. Bunk, and C. David, Nat. Phys. **2**, 258 (2006).
[11]A. Olivo and R. Speller, Appl. Phys. Lett. **91**, 074106 (2007).
[12]C. David, J. Bruder, T. Rohbeck, C. Grunzweig, C. Kottler, A. Diaz, O. Bunk, and F. Pfeiffer, Micro. Eng. **84**, 1172–1177 (2007).
[13]S. Rutishauser, M. Bednarzik, I. Zanette, T. Weitkamp, M. Börner, J. Mohr, and C. David, Microelectron. Eng. **101**, 12–16 (2013).
[14]A. V. Bronnikov, J. Opt. Soc. Am. A **19**, 472 (2002).
[15]D. Paganin and K. A. Nugent, Phys. Rev. Lett. **80**, 2586 (1998).
[16]K. Morgan, D. Paganin, and K. Siu, Opt. Express **19**, 19781–19789 (2011).
[17]R. Hofmann, J. Moosmann, and T. Baumbach, Opt. Express **19**, 25881–25890 (2011).
[18]J. Moosmann, R. Hofmann, and T. Baumbach, Opt. Express **19**, 12066–12073 (2011).
[19]J. Moosmann, R. Hofmann, A. V. Bronnikov, and T. Baumbach, Opt. Express **18**, 25771–25785 (2010).
[20]X. Wu, H. Liu, and A. Yan, Opt. Lett. **30**, 379–381 (2005).
[21]J.-P. Guigay, Optik **49**, 121 (1977).
[22]E. Bennett, R. Kopace, A. F. Stein, and H. Wen, Med. Phys. **37**, 6047 (2010).
[23]H. Wen, E. Bennett, R. Kopace, A. F. Stein, and V. Pai, Opt. Lett. **35**, 1932 (2010).
[24]A. Mozzanica, A. Bergamaschi, R. Dinapoli, H. Graafsma, D. Greiffenberg, B. Henrich, I. Johnson, M. Lohmann, R. Valeria, B. Schmitt, and S. Xintian, J. Instrum. **7**, C01019 (2012).
[25]S. Cartier, A. Bergamaschi, R. Dinapoli, D. Greiffenberg, I. Johnson, J. H. Jungmann, D. Mezza, A. Mozzanica, B. Schmitt, X. Shi, M. Stampanoni, J. Sun, and G. Tinti, J. Instrum. **9**, C05027 (2014).
[26]S. M. Sze, *Semiconductor Devices—Physics and Technology* (John Wiley & Sons, Zweite Auflage, 2002).
[27]A. Bergamaschi, Ch. Broennimann, R. Dinapoli, E. Eikenberry, F. Gozzo, B. Henrich, M. Kobas, P. Kraft, B. Patterson, and B. Schmitt, Nucl. Instrum. Methods Phys. Res., Sect. A **591**, 163–167 (2008).
[28]A. Bergamaschi, S. Cartier, R. Dinapoli, D. Greiffenberg, J. H. Jungmann-Smith, D. Mezza, A. Mozzanica, B. Schmitt, X. Shi, and G. Tinti, J. Instrum. **10**, C01033 (2015).
[29]R. Turchetta, Nucl. Instrum. Methods Phys. Res., Sect. A **335**, 44–58 (1993).
[30]A. Schubert, A. Bergamaschi, C. David, R. Dinapoli, S. Elbracht-Leong, S. Gorelick, H. Graafsma, B. Henrich, I. Johnson, M. Lohmann, A. Mozzanica, V. Radicci, R. Rassol, L. Schädler, B. Schmitt, X. Shi, and B. Sobott, J. Synchrotron Radiat. **19**, 359 (2012).
[31]M. Stampanoni, A. Groso, A. Isenegger, G. Mikuljan, Q. Chen, D. Meister, M. Lange, R. Betemps, S. Henein, and R. Abela, AIP Conf. Proc. **879**, 848 (2007).
[32]S. Cartier, A. Bergamaschi, R. Dinapoli, D. Greiffenberg, I. Johnson, J. H. Jungmann-Smith, D. Mezza, A. Mozzanica, X. Shi, G. Tinti, B. Schmitt, and M. Stampanoni, J. Instrum. **10**, C03022 (2015).